

Dynamic grouping of ongoing activity in V1 hypercolumns

Rui Zhang ^{a,1} , Jiayu Wang ^{a,1} , Xingya Cai ^a, Rendong Tang ^a, Haidong D. Lu ^{a,b,*}

^a State Key Laboratory of Cognitive Neuroscience and Learning, IDG/McGovern Institute for Brain Research, Beijing Normal University, Beijing, China

^b Department of Neurology, Zhongshan Hospital, Institute for Translational Brain Research, Fudan University, Shanghai, China

ARTICLE INFO

Dataset link: <https://data.mendeley.com/datasets/v6563pxdn9/1>

Keywords:

Macaque
V1, V2
Spontaneous activity
Neuron ensemble
Functional map
Two-photon calcium imaging
Functional connectivity

SUMMARY

Neurons' spontaneous activity provides rich information about the brain. A single neuron's activity has close relationships with the local network. In order to understand such relationships, we studied the spontaneous activity of thousands of neurons in macaque V1 and V2 with two-photon calcium imaging. In V1, the ongoing activity was dominated by global fluctuations in which the activity of majority of neurons were correlated. Neurons' activity also relied on their relative locations within the local functional architectures, including ocular dominance, orientation, and color maps. Neurons with similar preferences dynamically grouped into co-activating ensembles and exhibited spatial patterns resembling the local functional maps. Different ensembles had different strengths and frequencies. This observation was consistent across all hypercolumn-sized V1 locations we examined. In V2, different imaging sites had different orientation and color features. However, the spontaneous activity in the sampled regions also correlated with the underlying functional architectures. These results indicate that functional architectures play an essential role in influencing neurons' spontaneous activity.

1. Introduction

When we examine a single neuron, its spontaneous activity appears to be random. However, when more neurons are examined simultaneously, we found that neurons' spontaneous activity often correlate with each other, especially for neurons close-by (Leopold et al., 2003; Smith and Kohn 2008; Smith and Sommer 2013). The correlation strength varies with neurons' selectivity features and their locations (Maier et al. 2010; Okun et al. 2015). Such variation may due to the intrinsic cortical functional networks, like orientation maps (Arieli et al. 1995, 1996; Tsodyks et al. 1999; Singh et al. 2008; Cai et al. 2023). However, direct evidence for such dependency is still lacking. For non-human primates, there are many functional architectures in their sensory cortices. For example, there are orientation, color, and ocular dominance maps in area V1. In the hypercolumn model Hubel and Wiesel proposed, a column under a 1-mm²-sized surface contains full cycles for all these features (Hubel and Wiese 1974). How do these nested networks affect neuron's spontaneous activity? Whether a single neuron's activity is determined by the neuron's spatial location within these functional maps? The answers to these questions remain unknown.

Two-photon calcium imaging provides a way to image hundreds to

thousands of neurons within a mm²-sized cortical region. It has been used in studying spontaneous activity in different animal models, for example in mice (Goltstein et al. 2015; Mizuno et al. 2018), rats (Ch'ng and Reid 2010), cats (Ch'ng and Reid 2010), and ferrets (Smith et al. 2018). To our knowledge, there is no report of two-photon study of spontaneous activity in non-human primates. Previously, we used two-photon calcium imaging and studied neurons' visual response features (Tang et al. 2020). Here, we examined spontaneous activity with the same technique. We characterized neurons' spontaneous activity with respect to their spatial context in the local functional maps, as well as their selectivity to visual features. As a classical model for brain research, macaques have been studied on spontaneous activity in both micro (electrophysiology) and macro (fMRI) scales. Two-photon imaging has the unique resolution and scale to bridge these findings.

2. Results

In 3 macaques, we injected AAV virus to express GCaMP6s proteins in multiple locations in V1 and V2. A chronic optical chamber with a diameter of 13-mm was implanted (Fig. 1A&B). In the subsequent anesthetized experiments, we imaged calcium signals with a 16 ×

* Corresponding author at: State Key Laboratory of Cognitive Neuroscience and Learning, IDG/McGovern Institute for Brain Research, Beijing Normal University, Beijing, China.

E-mail address: haidong@fudan.edu.cn (H.D. Lu).

¹ These authors contributed equally to this work

objective. The frame size was 0.83×0.83 mm, collected at 1.3Hz frame rate. Imaging depth was 180–270 μm . In each experiment, imaging of spontaneous activity always started first, normally lasted for 70 min (~5000 frames), when the animal's eyes were closed. After that, visual responses of the same group of neurons were collected. Visual stimuli were drifting gratings of different colors and orientations, presented monocularly or binocularly. Each stimulus was presented for 2 ss. About 400–600 cells (average 569 cells) can be identified from each imaging site (e.g., Fig. 1C). Neuron's fluorescent activity time courses were filtered (0.005Hz Highpass), transformed to dF/F , and z-scored. Following results were all based on these $n \times m$ (cell number \times frame number) matrices (e.g., Fig. 1F).

In separate experiment, intrinsic signal optical imaging was also performed for these chambers and basic functional maps were obtained

for comparison with the functional maps obtained with two-photon imaging (Figure S1).

2.1. Basic features in spontaneous activity

In single neurons, spontaneous calcium signal appeared to fluctuate randomly (Fig. 1D), with an amplitude smaller than their visually driven responses (Fig. 1E). Population-wise, neurons showed burst-like co-activation (Fig. 1F). These bursts usually had different neuron participants, and some spontaneous frames had similar spatial patterns with the stimulus ones (i.e., functional maps, Fig. 1&J). This suggests that the spontaneous ensembles were not formed randomly, rather, they were formed by some internal mechanisms that resembled the stimulus effects. As a comparison, after each neuron's spontaneous activity was

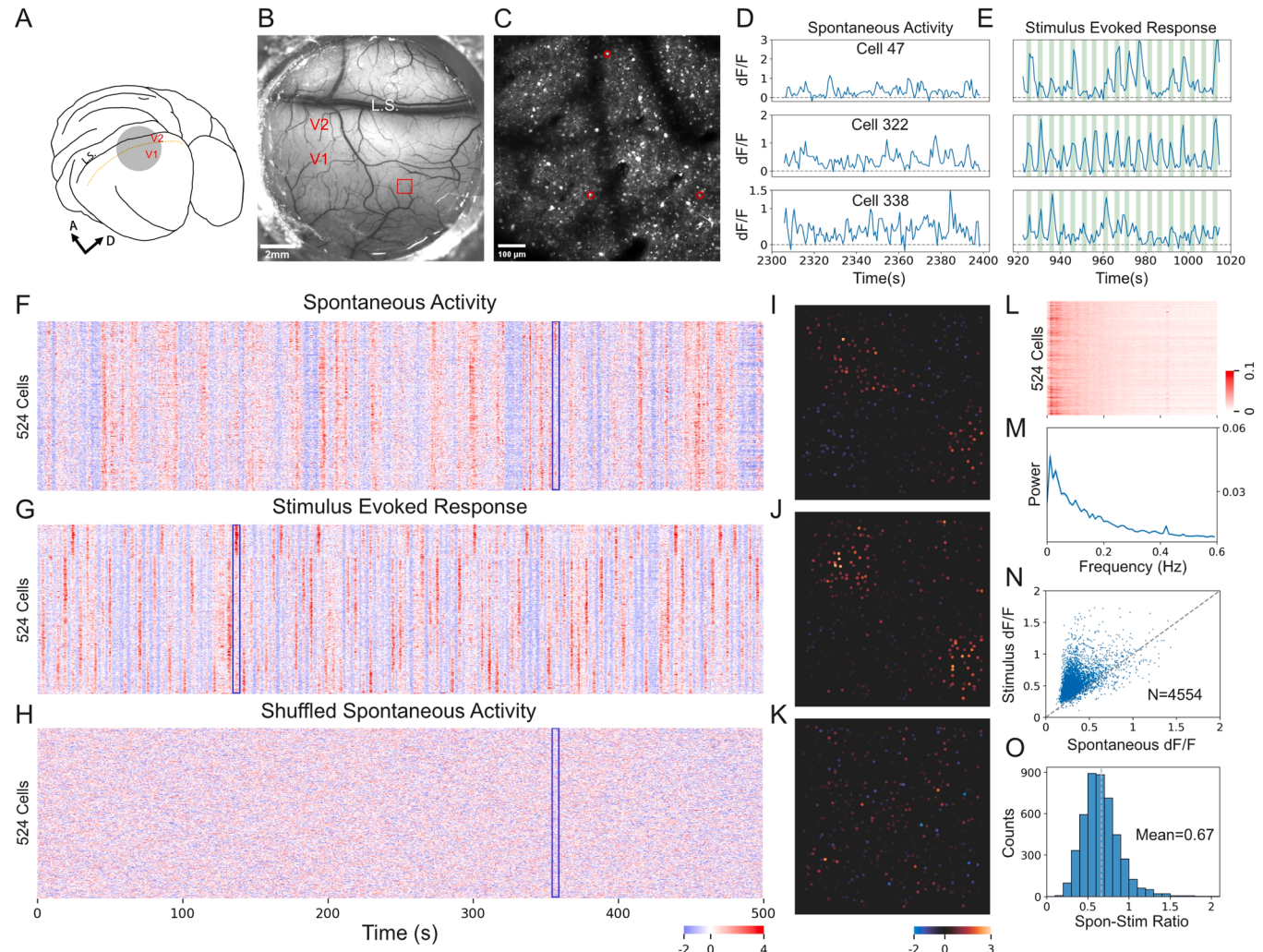


Fig. 1. Two-photon calcium imaging of spontaneous activity **A.** An illustration of the macaque brain and the imaging region (circle) over areas V1 and V2. A: anterior, D: dorsal. L.S.: Lunate sulcus. **B.** In vivo image of a 13-mm diameter optical chamber. The red frame indicates the size of a two-photon imaging site in V1. **C.** Fluorescent image of neurons in the red-frame region in panel B. This $830 \times 830 \mu\text{m}$ frame was imaged using a $16\times$ objective at a $197 \mu\text{m}$ depth from the cortical surface. Three neurons marked in red are examined in detail in panel D & E. **D.** Representative spontaneous activity (dF/F) of the 3 example neurons marked in C. Individual neurons showed random activity. **E.** Representative responses to visual stimuli of the same example neurons shown in D. Vertical green bars indicate the stimulus presentation time. The visual stimuli were gratings of various orientations. **F.** Spontaneous activity of all neurons ($N = 524$) imaged in site 1 over a period of 500 ss. Neurons' activity was individually normalized. Example frames (blue outline) were examined in detail in panel I. **G.** Responses of the same group of neurons in F to gratings presented at various orientations. **H.** The same spontaneous data as in F but were phase-shuffled for each individual neuron. **I.** An average of 6 consecutive frames (outlined in F) showing the Z values of all neurons at that time point. Only the neurons were shown in this frame. The active neurons exhibited a spatial pattern which was similar to one obtained in stimulus runs. **J.** An average of example frames (outlined in G) extracted from a stimulus run showing the pattern of co-activating neurons. **K.** Example frames (outlined in H) from the shuffled data did not exhibit a meaningful modular pattern. **L.** Frequency spectrums of all neurons in this site. Signals below 0.005Hz were removed in data preprocessing. The peak at 0.42 Hz represents the respiration frequency of the animal. **M.** Average power spectrum exhibited major signals under 0.1Hz. **N.** Average amplitudes of responses to stimulus and average amplitudes of spontaneous activity for all the neurons imaged in 8 V1 sites ($N = 4554$). **O.** Distribution of spontaneous-stimulus response amplitude ratios for all neurons.

phase-shuffled, the overall pattern was completely different (Fig. 1H) and no such spatial patterns could be found (e.g., Fig. 1K). Single-neuron-wise, their spontaneous activation rates were similar, in a range of 0.01~0.05Hz (Fig. 1L&M). Their average fluctuation amplitude was about 67 % of that under visual stimulation (Fig. 1N&O). Population-wise, spontaneous ensembles were dynamically formed at a mean frequency of 0.15 Hz, each ensembles lasted ~3 ss (Fig. S2C). Both ensemble and single cell events exhibited lower burstiness compared to a random distribution, suggesting that spontaneous events were more

uniformly distributed in time (Fig. S2 E&I). Ensemble sizes (number of neurons co-activated) and frequencies (how frequent that size of ensemble observed) were negatively correlated (Fig. S2C).

2.2. Orientation patterns in population activity

PCA (Principal Component Analysis) is a useful data-driven analysis tool and frequently used in fMRI data analysis (Carbonell et al. 2011). For the high-order spontaneous data, we used PCA to reduce its

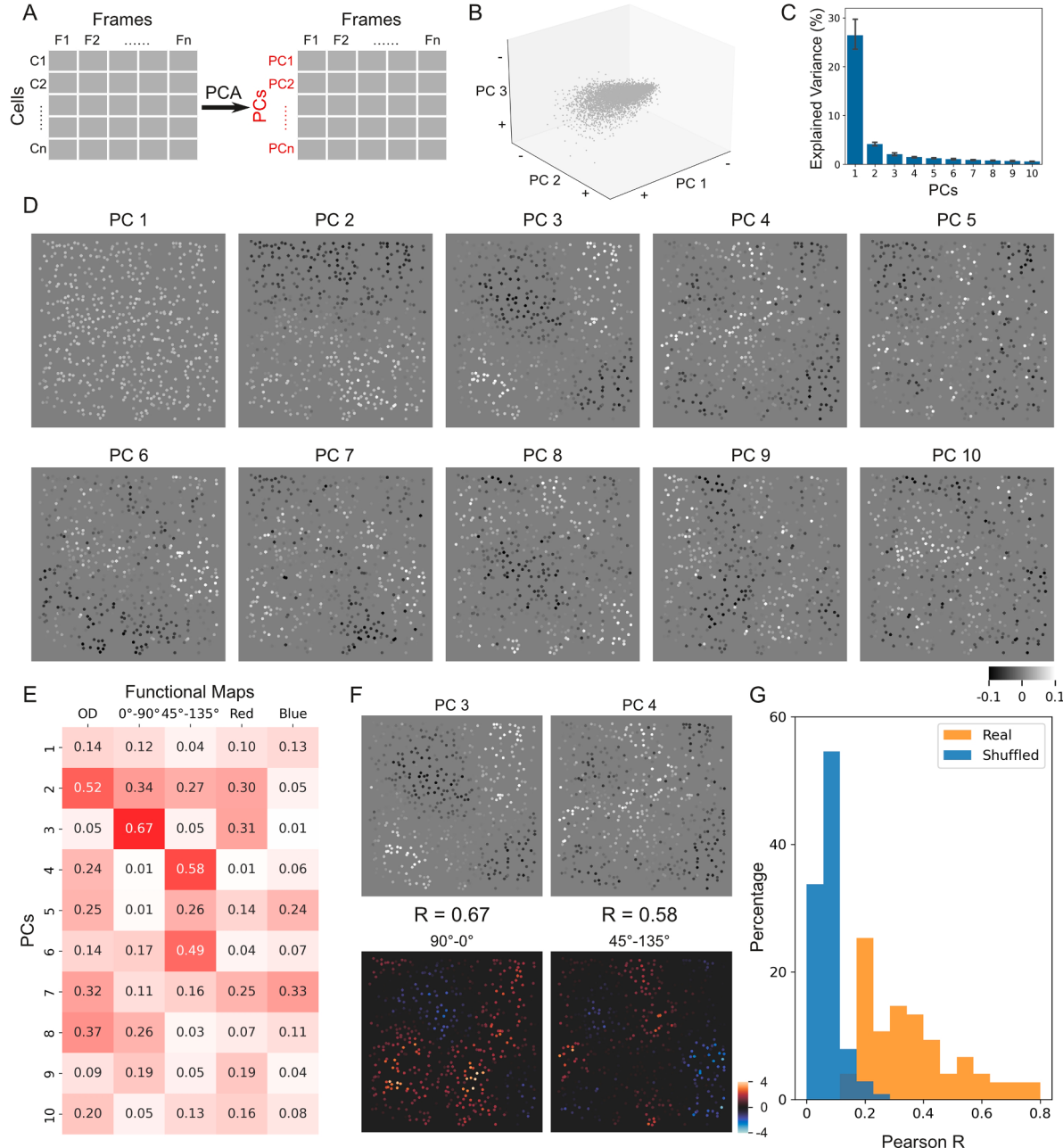


Fig. 2. Spontaneous PCA results in cell space **A**, Illustration of spontaneous data structure and PCA. Spontaneous activity data were organized into two-dimensional matrix: cell dimension and frame dimension. PCA was then carried out in the cell dimension and resulted hypothetical neurons as PCs (cell PCs). **B**, All spontaneous frames from one example site plotted in the PC space. **C**, Percentages of the response variance accounted for by the top 10 PCs. **D**, Visualization of the top 10 PCs, each was a weight map representing the different weights of the original neurons on this PC. **E**, Correlation matrix between the PCs and functional maps of the site. Many PC had similar patterns with the functional maps. **F**, Two PCs (same as shown in D) having the highest correlation scores (in E) are shown (top) along with their best-matching functional maps (bottom). **G**, Distribution of all the correlations between PCs and functional maps (blue, calculated from all 8 V1 sites), compared with the distribution of the same correlations calculated for shuffled data (orange). Each PC contributed one correlation value (the best correlation); thus total 80 correlations were plotted (real). For the shuffled data, each spontaneous data was shuffled 500 times, and 80 correlation values were obtained for each shuffle.

dimensionality. As illustrated in Fig. 2A, PCA reduced the dimension in cell axis. After PCA, the top 10 principal components (PCs) explained $39.4 \pm 5.6\%$ of the total variance (averaged from all 8 V1 sites, Fig. 2C), indicating the effectiveness of this procedure. Fig. 2B shows the PC space and spontaneous data from an example site, which contained 5352 frames collected in ~ 70 min. Each data point represents a frame. The data points were mainly clustered into one cloud, without separate clusters. This suggests that there were no separate dominate states in the imaging period. After dimension reduction along the cell axis, each PC can be viewed as a hypothetical cell, whose activity was a weighted sum of the activity of the original neurons. Each PC thus can be visualized as a frame of the cell weights (e.g., Fig. 2D). PC1 appeared to be a global pattern, in which all neurons had a high weight. Indeed, its timecourse was almost identical to the sum of all neurons' z-scored activity

(Fig. S3B). It accounted for $26.4 \pm 4.5\%$ variance in the data, indicating that the co-activation of neurons in the whole imaging region was the most dominant component in the spontaneous activity. The rest of PCs explained much less of the total variance, but each had a spatial pattern, some of them resemble the orientation map in that region (Fig. 2E&F), others had a better correlation with ocular dominance or color maps (Fig. 2E). These correlations were significantly higher than those obtained with shuffled data (Fig. 2G).

As a control, we phase shuffled each neuron's spontaneous activity (the same as in Fig. 1H), and did the same PCA on the shuffled data. The result PCs had a very low power in accounting for the total variance (top 10 PCs explains a total of $3.2 \pm 0.5\%$ of the variance, Fig. S4B). Neither did the visualized PCs have systematic pattern or correlate with functional maps (Fig. S4 C&D). This supports that the patterns we observed

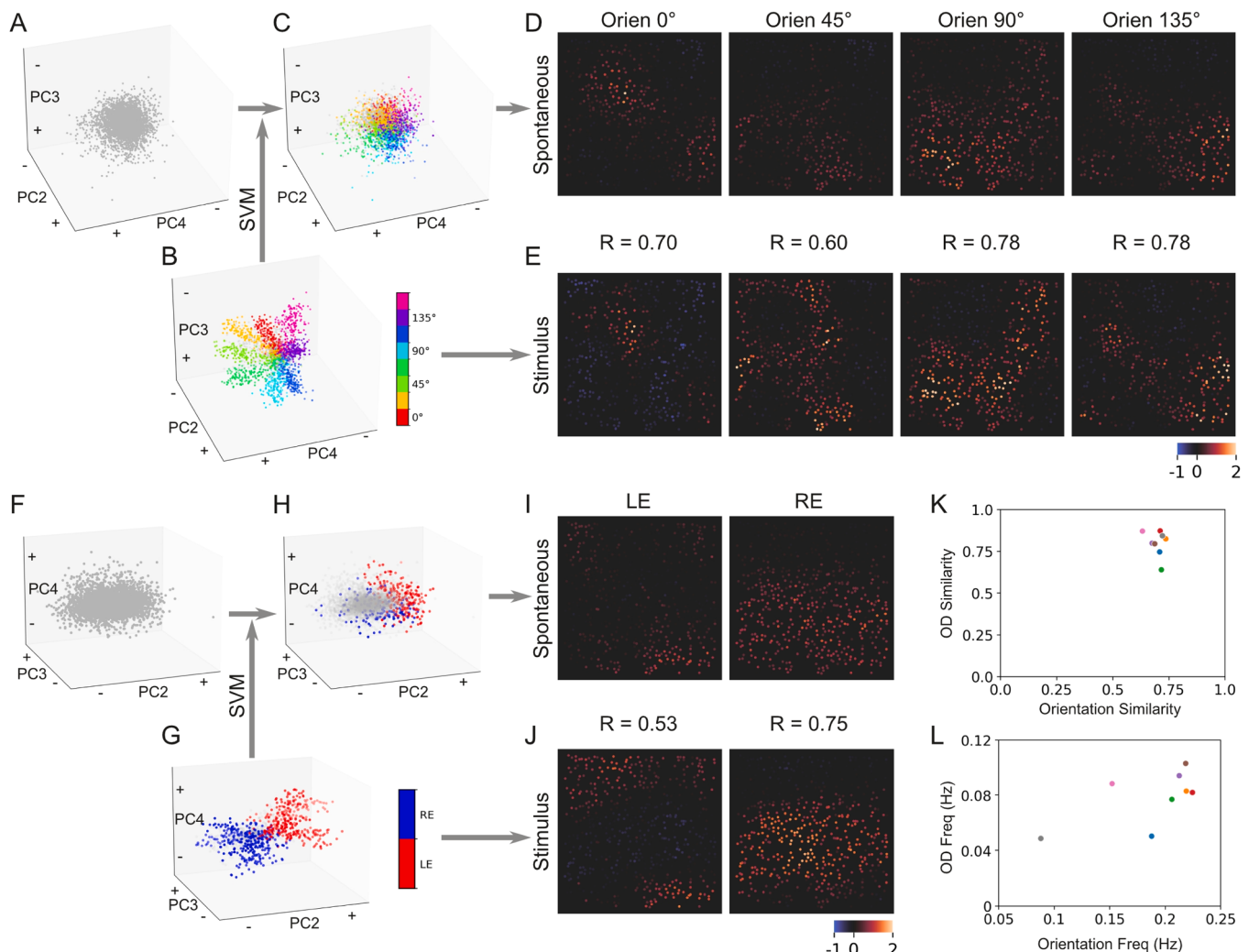


Fig. 3. Spontaneous orientation and OD patterns in V1. A. Spontaneous frames in the PC space shown with axes of PC2, PC3, and PC4. This case is the same as the one shown in Fig. 2B. B. Stimulus-driven frames plotted in the PC space resulted from PCA on spontaneous data (i.e., the same space as in A). Gray dots are frames imaged during inter-stimulus-intervals (ISI). The coordinates of the frames were used to train a SVM classifier to categorize stimulus orientations (different colors). C. The same plot as in A except that frames were colored based on the SVM classification of these spontaneous frames. Different colors represent different orientation categories that are the same as in B, and gray ones were classified as non-orientation category (ISI frames). D. Averages of the same-category frames in C. These maps had high correlations with those functional maps obtained from stimulus-driven images (E). E. Stimulus-driven orientation maps (single-condition maps). F-J. The same analysis as in A-E, but on ocular dominance features. F. The same spontaneous frames in the PC space shown with axes of PC3, PC4, and PC2 (same data as in A). G. Stimulus-driven frames collected in monocular stimulation runs plotted in the spontaneous PC space (same space as in F). Red, Blue and gray dots represent left-eye, right-eye, and ISI frames, respectively. Their coordinates were used to train a SVM classifier to separate left-eye, right-eye, and ISI frames. H. Spontaneous frames as in F and colored according to the SVM classified categories. I. Left-eye (LE) and right-eye (RE)-patterns obtained from the classified spontaneous frames. They had a good correlation with the functional maps in J. J. Left- and right-eye functional maps obtained from stimulus-driven frames. K. Orientation and ocular dominance correlation values, as shown in D&E and I&J, for 8 imaged V1 sites. These values were similar across different V1 sites. L. Occurrence frequencies of orientation ensembles and ocular dominance ensembles, which were correlated across 8 imaged V1 sites.

in spontaneous data were non-random in nature.

Since the PC axes contained orientation features (Fig. 2E&F), we can verify this by plotting orientation response data into this PC space. We plotted cells' responses to gratings (new data) into the PC space obtained in spontaneous data analysis (old space). As we can see, frames obtained with 8 different grating orientations (different colors) clustered into 8 different branches with neighboring branches representing neighboring orientations (Fig. 3B). This proves that the space is indeed organized with respect to the orientation information.

Now with the coordinates of orientation frames in the PC space, we can further examine whether spontaneous frames can be classified into different orientation groups. We trained a SVM classifier using the PC coordinates of the orientation frames (Fig. 3B). We only used the coordinates of the first 10 PC axes and achieved 85.8 % correct rate (5-fold cross validation) in the 9-category classification (8 orientations and 1 blank). We then used this classifier to examine the spontaneous frames. There were 23.2 % frames that were classified as orientation frames, the rest (76.8 %) were classified as blanks (Fig. 3C). Compared with the separate branches in stimulus frames (Fig. 3B), the spontaneous frames were more continuous (Fig. 3C), indicating a more uniform orientation representation in the spontaneous activity. PC 2, 3, and 4 had the largest contribution in the SVM classification, therefore were used to visualize the PCA results (Fig. 3A-C). Finally, the averaged spontaneous frames in each orientation category were very similar to those obtained from stimulus frames (Fig. 3D&E), and had higher correlation values than the controls obtained with artificial stimulus data (Fig. S5). The correlation was around 0.7, which further confirms the existence of orientation-specific co-activation in these neurons. Although PC1 represented global activity and did not contribute to specific orientation patterns, frames had higher PC1 wt tended to have higher chance to be classified as an orientation pattern (Fig. S3 D&E).

2.3. Ocular dominance and color patterns in spontaneous activity

During each experiment, we also collected neurons' responses to monocular black/white grating, as well as responses to binocular color gratings. We used the same approach and plotted these stimulus-driven data (frames) into the old PC space obtained with spontaneous data (i.e., same as Fig. 2B). Fig. 3G shows that the frames collected during left-eye stimulation (red) and right-eye stimulation (blue) were well separated in the PC space. A SVM classifier trained with the coordinates of these frames subsequently identified 6.8 % of the spontaneous frames as monocular activation frames (Fig. 3H). The results were confirmed by the similarity between the averaged spontaneous frames and left- or right-eye functional maps (Fig. 3I&J).

We also examined whether color response patterns existed in the spontaneous activation. With the same method, we found some spontaneous frames can also be classified as similar to those obtained in color grating stimulation (Fig. S6C). However, the averaged color spontaneous patterns had weaker similarity with the color functional maps (Fig. S6 D&E), the correlation values ranged from 0.15 to 0.59 (Pearson's $r = 0.41 \pm 0.11$ overall). We conclude that although co-activation of color-selective neurons did exist in spontaneous activity, it was not as robust as those for orientation and ocular dominance ones. This is consistent with our previous findings obtained with intrinsic optical imaging (Cai et al. 2023).

So far, spontaneous patterns were only exhibited in form of neurons (Fig. 3D&I, Fig. S6D). We also examined corresponding spontaneous patterns in form of frames (Fig. S7), in which original dF/F frames of the classified frames were averaged. Although the correlation scores were lower, the overall similarity was evident for corresponding spontaneous patterns and functional maps (Fig. S7).

From each of 8 V1 imaging sites, we obtained clear orientation and ocular dominance patterns in spontaneous activity. These patterns had an average correlation value of 0.8 with corresponding functional maps. Variation among imaging sites were small (Fig. 3K). As a comparison,

correlation value for color pattern is 0.41. The occurrence frequency of these patterns varied from experiment to experiment (Fig. 3L), which may due to different anesthetic statuses of the animals in each experiment. The frequencies for orientation and ocular dominance in one experiment were normally correlated (Fig. 3L), which is consistent with this hypothesis. In summary, these observations indicate that neurons with common preferences co-activated not only during visual stimulation, but also in ongoing activity.

2.4. Correlated activity among similarly tuned neurons

So far, we did PCA dimensional reduction in *cell* dimension. Similarly, we did PCA in *frame* dimension in order to see whether cells may cluster based on this data-driven approach. As shown in Fig. 4A, each PC axis represents one frame, and each data point in the frame space is a cell. The dimensionality of this frame space was higher, as the top 20 PCs only explained $25.3 \pm 3.5\%$ variance (Fig. 4B). However, we observed a separation of different orientation-preferring neurons (Fig. 4C), as well as separations of left-eye and right-eye preferring neurons in this PC space (Fig. 4D). This indicates that neurons with common tuning preferences had similar spontaneous activation, and that these tuning features (ocular dominance, orientation) were among the top factors that influenced neurons' spontaneous activity (among the top PCs).

We calculated average vectors for neurons preferring 0° and 90° and vector for neurons preferring 45° and 135° (arrows in Fig. 4C). Visualization of these vectors exhibited orientation patterns (Fig. S8A&B). These two vectors were orthogonal to each other in this high-dimensional PC space (Fig. S8D). In addition, these two vectors were both orthogonal to the vector for ocular-dominance neurons (arrow in Fig. 4D, also see Fig. S8D). These observations indicate that these factors had orthogonal influences on neurons' spontaneous activity, and different functional networks had independent activity, did not affect each other.

These results can also be directly obtained by calculating pair-wise correlations between neurons' spontaneous activity. Although most neurons were positively correlated (due to the global signal), the degree of correlation varied. Fig. 4E shows that correlation dropped when the distance between neurons increased. The highest correlation occurred in neuron pairs within a short distance ($\sim 200\mu\text{m}$, Fig. 4E). This value is comparable to the average size of basal dendritic spread of neurons in V1, as well as the size of terminal patches of V1 neuron axons (Lund et al. 1993; Lund and Wu 1997). Fig. 4F shows that neurons with similar orientation-preferences had stronger correlation. Fig. 4G shows that neurons with similar eye-preferences had stronger correlation. Neurons with weak eye-preferences (binocular neurons) or neuron pairs had different eye preferences had weaker correlations.

2.5. Spontaneous activity in V2

We also imaged 3 sites in area V2. The 3 sites sited in different locations with respect to V2 stripes, as indicated by functional maps obtained with intrinsic signal optical imaging (Fig. S1). Unlike V1 neurons, neurons in V2 are mostly binocular and have no/weak eye preferences. In addition, different stripes exhibit large differences in orientation selectivity and color selectivity. We did the same analysis for the V2 data. Fig. 5A shows the data from a site located in a thick/pale stripe. This site had strong orientation selectivity and weak color selectivity. Accordingly, orientation patters obtained from its spontaneous activity was strong (Fig. 5E), but color was weak (not shown). Fig. 5F shows data from another V2 site, which was located in a thin stripe. The spontaneous activity in this site exhibited strong color patterns (Fig. 5J). The correlation value (~ 0.5) was higher than all those observed in V1 (Fig. 5K).

Thus, like in V1, spontaneous activity in V2 also exhibited patterns that were correlated with the underlying functional architectures. There were also differences between these two areas. For example, V2 had

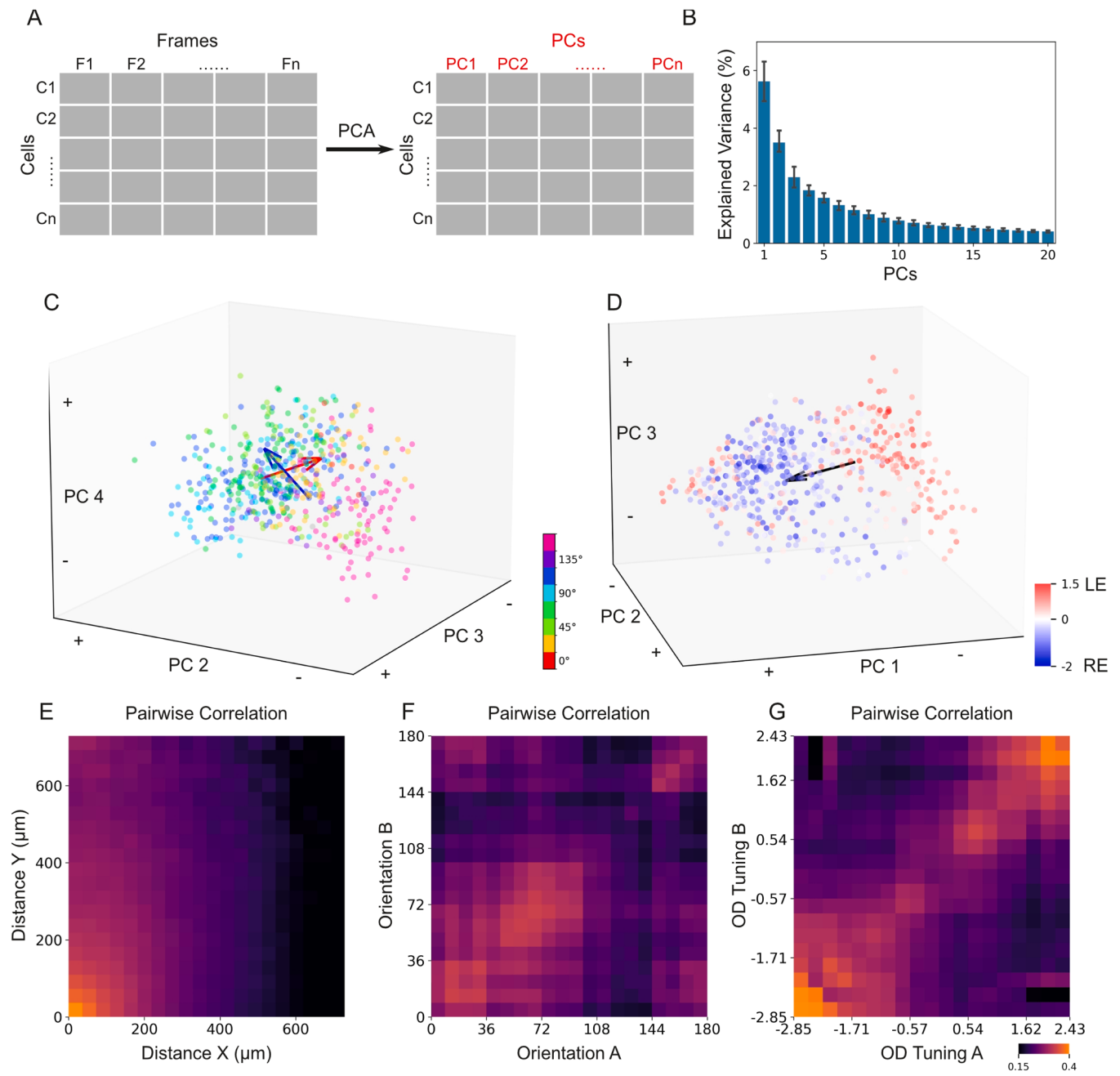


Fig. 4. Spontaneous PCA results in frame space **A**. Similar to Fig. 2A, but PCA was carried out along the frame dimension and resulted hypothetical frames as PCs (frame PCs). **B**. Percentages of the response variance accounted for by the top 20 PCs. **C**. Neurons in the PC space colored according to their orientation preferences. Red arrow is a 0° vs. 90° vector, which starts from the mean location of all the 90°-preferring neurons and points toward the mean location of all the 0°-preferring neurons. Similarly, blue arrow represents the 45° vs. 135° vector. These two vectors are orthogonal to each other. **D**. Same plot as in C but colored according to neurons' ocular dominance preferences. The black arrow represents the LE vs. RE vector, which is also orthogonal to the orientation vectors shown in panel C. **E**. Pairwise correlations between the responses time courses of any two different neurons. The correlation values were sorted and averaged according to the distances of the two neurons. **F**. Same as in E, but sorted with neurons' orientation preferences. **G**. Same as in F and E, but sorted with neurons' ocular dominance preferences.

stronger color spontaneous patterns than V1. In addition, 3 imaged V2 regions had very different features, due to the small imaged regions and large V2 functional architectures. In V1, the 8 imaged regions had similar properties, indicating that the imaged regions had a scale close to the functional element of V1, the hypercolumn.

3. Discussion

We analyzed spontaneous activity of population neurons in V1 and V2 in anesthetized macaques. We found that neurons dynamically

formed different active ensembles. The ensembles resembled the known functional architectures, including different orientation-preference patterns, ocular dominance and color patterns. As a result, neurons had common selectivity tended to have higher correlated activity. In V1, orientation and ocular dominance both had strong effect on neurons' spontaneous activity, while color's effect was weaker. In V2, depending on the particular locations, orientation and color could have strong or weak effects on neurons' spontaneous activity. These results provided direct evidence for the hypothesis that spontaneous activity depends on underlying functional architectures. Different architectures have

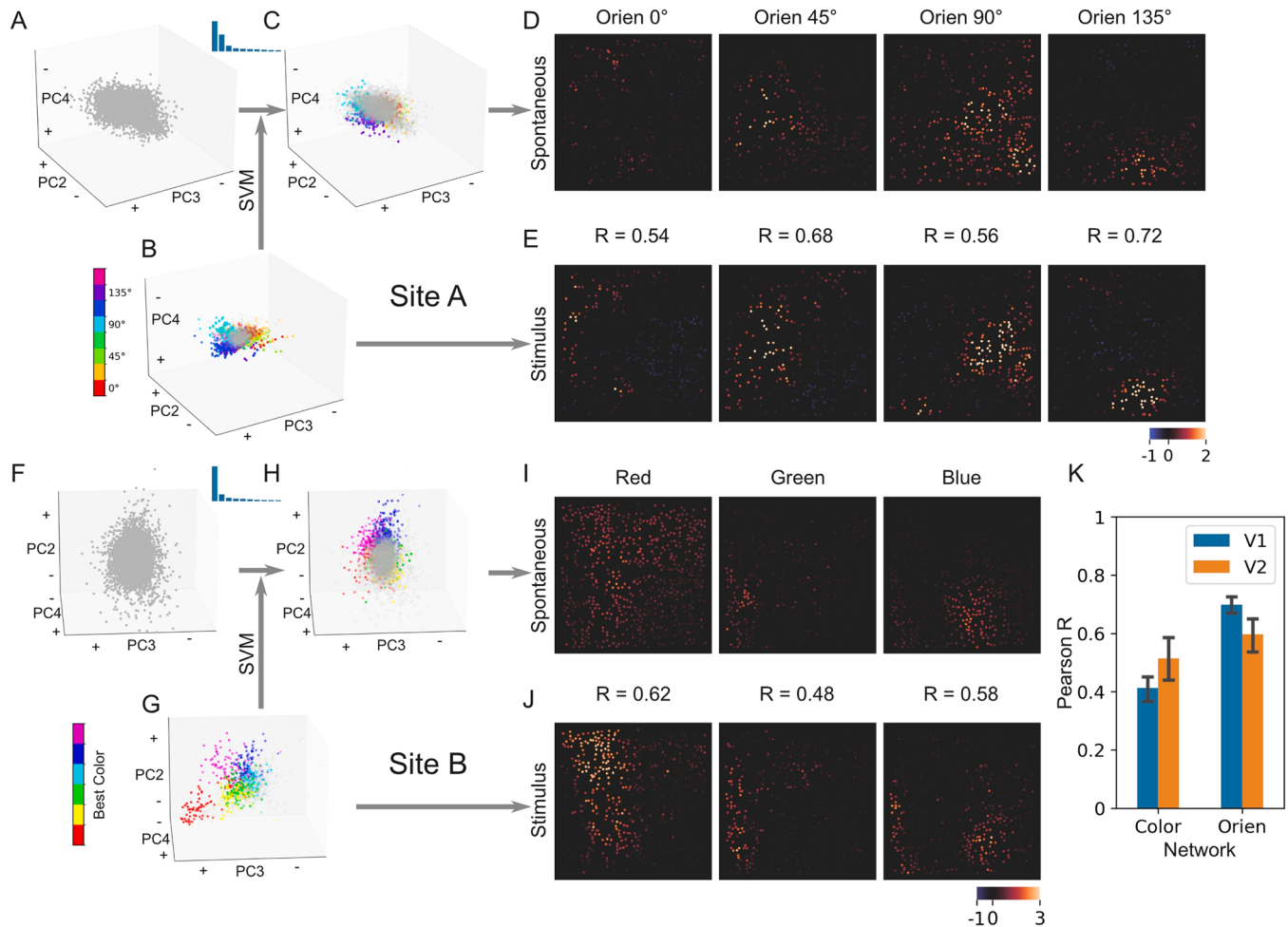


Fig. 5. Spontaneous orientation and color patterns in V2 A-E. Similar to the PCA and SVM classification procedures shown in Fig. 3, but for a V2 site. Similar to V1, spontaneous orientation patterns were observed (E). Bar plot represent top 10 PC's explained variance ratio. F-J. Similar to above, but for another V2 site. This V2 site had weak orientation selectivity, but strong color selectivity. The spontaneous color patterns (K) were observed and well correlated with functional maps (L). K. Correlation values between spontaneous patterns and functional maps for all 3 V2 imaging sites (orange) compared with those from V1 (blue).

different contributions. Further, the neuronal evidence supports previous findings obtained with voltage-sensitive-dye imaging (Omer et al. 2019) and hemodynamic imaging (Cai et al. 2023) and proved the neural origin of the mesoscopic functional connectivity they observed.

3.1. Preferential horizontal connection model for patterned spontaneous activity

These functional-architecture-like activation patterns can be explained largely by non-uniform horizontal connections. Previous studies have demonstrated preferential horizontal connections among neurons having similar tuning properties, including orientation preferences (Gilbert and Wiesel 1989; Kisvarday et al. 1997), ocular dominance (Malach et al. 1993; Yoshioka et al. 1996), and color preferences (Livingstone and Hubel 1984; Yoshioka et al. 1996; Yabuta and Callaway 1998). These domain-specific connections coexist with a large amount of domain-non-specific connections, which connect nearby neurons within a region comparable to the coverage of morphological spread of the neurites ($\sim 200\mu\text{m}$; Lund et al. 1993; Lund and Wu 1997; Malach et al. 1993; Yoshioka et al. 1996). The strong pair-wise correlation in short distance (Fig. 4E) is consistent with these short domain-non-specific connections. These horizontal connections are the morphological basis for the correlated ongoing activity.

As illustrated in the conceptual model in Fig. 6, spontaneous activity in V1 is influenced by both external inputs (e.g., LGN, V2) and intra-

areal connections (drawn based on currently available knowledge). The domain-non-specific connections (gray lines in Fig. 6C) are the morphological basis for the global activity we observed (PC1 in Fig. 2); and domain-specific connections among different types of functional domains (blue and red lines in Fig. 6C) are the basis for the multiple spontaneous patterns (e.g., PC2 in Fig. 2). A single V1 neuron normally located in the junction of multiple types of networks (OD, orientation, color) and fires when it receives enough inputs from earlier level and horizontal connections. Its activation also has non-uniform impact with its surrounding neurons through these non-uniform connections. Two types of connections are normally co-activated, as we have shown that the strengths of PC1 and PC2 are correlated (Fig. S3D). It has been shown that, comparing to spontaneous fluctuations around a single background state, such multi-state spontaneous activity is often slow and low-dimensional (Goldberg et al. 2004), which is consistent with our observations. Besides horizontal connections, spontaneous activity in LGN will also affect V1 activity, as well as those from top-down feedbacks (Fig. 6). However, blocking retinal or LGN input does not eliminate these patterned spontaneous activity (Chiu and Weliky 2001; Smith et al. 2018). In addition, feedback from higher-level cortices is normally feature-non-specific (Stettler et al. 2002). Thus, although these two factors may contribute to the global component, they are not necessary for the patterned spontaneous activity. The horizontal connections play a main role in these spontaneous patterns.

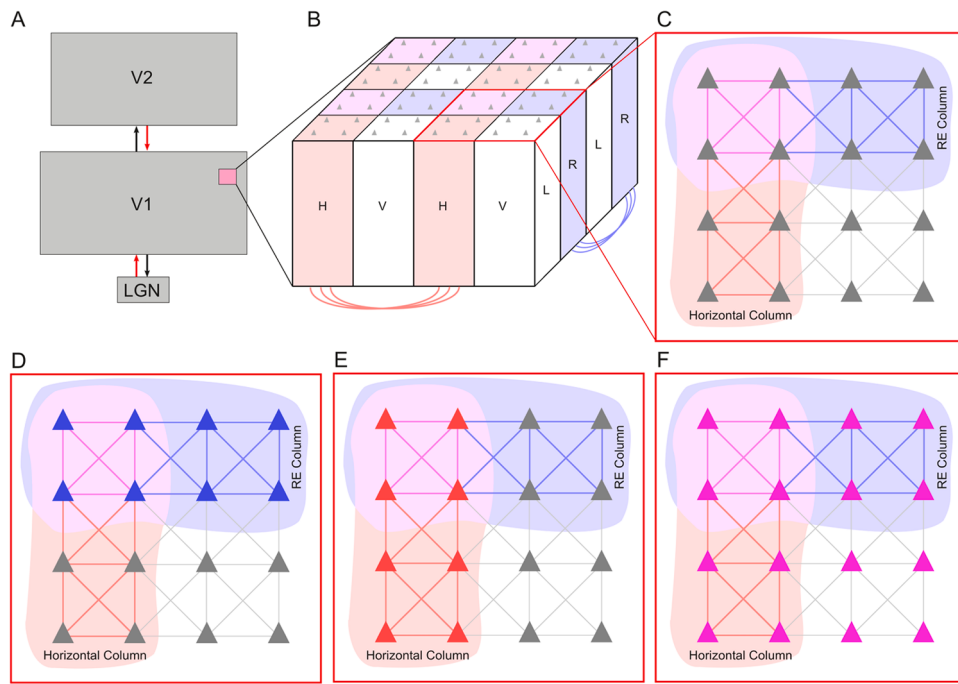


Fig. 6. Horizontal connection model A. Diagram of the visual processing pathway. Spontaneous activity in V1 is influenced by horizontal connections within V1 and interareal influences from LGN and higher visual areas (e.g., V2), indicated by red arrows. B. A simplified hypercolumn containing left- and right-eye columns (L, R), and horizontal and vertical orientation columns (H, V). Triangles represent neurons. Red and blue lines illustrate domain-specific connections that preferentially connect domains with common selectivity features. C. Surface view of a hypercolumn. Different types of horizontal connections are illustrated, including domain-specific connections among right-eye-preferring neurons (blue lines), horizontal-orientation-preferring neurons (red lines), and domain-non-specific connections (gray lines). D. Coactivation of right-eye-preferring neurons (blue triangles). E. Coactivation of horizontal-orientation-preferring neurons (red triangles). F. Coactivation of all neurons within the hypercolumn (pink triangles).

3.2. Spontaneous patterns are ubiquitous

Two-photon calcium imaging has been used in studying spontaneous activity in many species. For example, in mice (Goltstein et al. 2015; Mizuno et al. 2018) and rat (Ch'ng et al. 2010), it has been shown that neurons with common sensory information preference tend to synchronize. Common preference neurons also have stronger interconnections (Ko et al. 2011) that are formed in a stimulus-dependent manner after eye opening (Ko et al. 2013). These internally generated patterns often have a similar structure to stimulus-evoked ones (Mohajerani et al. 2013; Luczak et al. 2015). In awake mice, spontaneous patterns in sensory cortex also encode animal's spontaneous behavior, like facial movements (Stringer et al. 2019). In ferrets (Smith et al. 2018; Mulholland et al. 2021) and cats (Ch'ng et al. 2010), spontaneous orientation maps have been observed. In this study, we observed spontaneous ocular-dominance and color maps, in addition to orientation maps. Thus, this appears to be a cross-species common feature.

Correlations between spontaneous activity and functional architectures were also observed in other sensory cortices. For example, multi-electrode recordings have shown such evidence in rat auditory cortex (See et al., 2018); ECoG recordings in macaque area STP revealed a tonotopic organization in spontaneous activity (Fukushima et al., 2012); intrinsic signal optical imaging of spontaneous activity in somatosensory and motor cortices also revealed functional connections (Card et al. 2022). In higher level areas, for example PFC, spontaneous activity has revealed sub-regions (Kiani et al. 2015). Thus, the dependence of spontaneous activity on functional architecture has been observed in different areas, and in different species. Since these two factors are highly correlated, we suggest that unknown patterns in spontaneous activity could serve as an indicator for new functional architectures. This has important methodological meaning for studying high level areas, which are usually too complex to be studied with classical stimuli or

tasks.

3.3. Methodological comparisons

The present results support our previous findings obtained with intrinsic signal optical imaging (Cai et al. 2023). Both studies used the similar experimental procedures. Both found 3 types of spontaneous patterns in V1, in which orientation and ocular dominance patterns are strong, and color ones are weaker. In the two studies, spontaneous events have similar width (intrinsic signal: ~4 s, calcium signal: 3 s in Fig. S2D), and temporal frequencies (intrinsic signal: 0.02–0.03Hz, calcium signal: <0.1Hz in Fig. 1L&M). Thus, the present results support the neural origin of FC observed with hemodynamic signal, as well as the usefulness of such signals in study mesoscopic FC (Vasireddi et al. 2016; Card et al. 2022; Cai et al. 2023).

Functional MRI revealed large-scale, long-distance FC in the brain (Fox and Raichle 2007). Limited by its spatial resolution, fMRI is unable to detect sub-millimeter FCs, such as FCs between V1 orientation modules. Optical imaging methods such as VSD, ISOI and wide-field fluorescent imaging are useful in revealing FCs in the mesoscopic scale, but are unable to correlate with single-neuron activity. Two-photon imaging provides a good combination of both spatial and temporal resolutions, makes it an important tool in study fine-scale FC. Our results not only showed mesoscale FCs, but also revealed a global signal (PC1) that all neurons in the field of view contributed. This global signal had a slow temporal frequency (<0.1Hz, Fig. 1L&M), which may correspond to the infra-slow activity observed in fMRI (Fox and Raichle 2007) or wide-field calcium imaging (Mitra et al., 2018), providing a cellular-level support for the resting state BOLD signal.

3.4. Limitation of the present study

This study was carried out on anesthetized animals. Although it has

been shown that there are similar FC patterns in both anesthetized and awake animals (Vincent et al. 2007), some studies have also revealed that in anesthetized animals, spontaneous patterns were stronger (Omer et al. 2019). In addition, the type of anesthesia drug may also affect the strength of FC observed (Muta et al., 2023). Recent large-scale recordings in awake animal revealed more complex (higher dimensional) spontaneous activity, some may be related to animal behavior (review in Avitan and Stringer 2022). These behavioral or cognitive factors are more variable and add additional complexity into spontaneous signals. Spontaneous signals in anesthetized animals are simpler and easier to analyze and provided a baseline for further investigations. Signal-wise, the calcium signals we examined were slow and contained sub-threshold neuronal activity, which were different from spike signals. Finally, the PCA analysis detects the common activity in neuron population, thus single neuron characteristics were not examined in this study.

4. Materials and methods

4.1. Animals

Three adult macaque monkeys (two *Macaca mulatta*, one *Macaca fascicularis*, Beijing Inst. of Xieerxin Biology Resource and Hubei Top-gene Biotechnology Co., Ltd.) were imaged in this study. All procedures were performed in accordance with the National Institutes of Health Guidelines and were approved by the Institutional Animal Care and Use Committee of the Beijing Normal University (protocol number: IACUC (BNU)-NKCNL2016-06).

4.2. Surgery procedures

Animals were sedated with ketamine (10 mg/kg) or Zoletil 50 (tiletamine HCl and zolazepam HCl, 4 mg/kg). They were placed on a stereotaxic and artificially ventilated with isoflurane (1.5–2.5 %). A 22–24 mm diameter circular craniotomy and durotomy were performed in order to expose portions of areas V1 and V2. The craniotomy center was 18 mm from the midline, 14 mm from the posterior bone ridge (Fig. 1A).

In each case, we injected AAV9.Syn.GCaMP6S.WPRE.SV40 (#100843, titer $\geq 1 \times 10^{13}$ vg/mL, Addgene) into 10–15 cortical locations (520 nL each location) at a depth of 600–800 μm . Cortex was then protected with a piece of artificial dura, the retracted dura was covered back and glued to the top of the artificial dura with medical adhesive. The original bone piece was placed back, secured with a titanium mesh and bone screws. The scalp was sutured. After at least 8 weeks of virus expression, a second surgery was performed. The old craniotomy was reopened, a second round virus injections were performed, followed by implanting of an optical titanium chamber (inside/outside diameters: 13/15 mm).

4.3. Two-photon calcium imaging

After the animal recovered from surgery, two-photon calcium imaging was performed every 7–10 days. Animal preparation was the same as those in the surgery experiments, except that animal's head was tilted for $\sim 45^\circ$ to align with the fixed vertical imaging axis.

Anesthesia was switched from isoflurane to i.v. infusion of a mixture of propofol (2 mg/kg for induction and 2 mg/kg/hr for maintenance) and sufentanil (0.15 $\mu\text{g}/\text{kg}$ for induction and 0.15 $\mu\text{g}/\text{kg}$ /hr for maintenance). The animal was immobilized with vecuronium bromide (0.25 mg/kg for induction and 0.05–0.06 mg/kg/hr for maintenance) to prevent eye movements. Anesthetic depth was assessed continuously via monitoring the electrocardiogram, end-tidal CO_2 , blood oximetry, and body temperature. In order to have a stable anesthesia level, imaging usually started more than one hour after the anesthesia switch.

In each imaging experiment, spontaneous imaging session was always performed before the visual stimulus sessions. The monkey's eyes

were closed and covered with an additional eye-cover. The excitation wavelength of the laser (generated by Chameleon Ultra II, Coherent Inc) was set at 980 nm. Under a 16 \times objective (0.8 N.A., Nikon), 515 \times 512 pixel images, covering an $830 \times 830 \mu\text{m}$ cortical surface, were collected continuously at a frame rate of 1.3 Hz (Bruker Ultima IV Extended Reach, Bruker Nano Inc). Image plane was at a depth of 180–270 μm . Spontaneous imaging session usually lasted for 1–2.5 hr, during which we tried to maintain a stable environment with minimum light and sound.

After spontaneous imaging, the monkey's eyes were opened. Pupils were dilated (tropicamide) and fit with contact lenses of appropriate curvatures to focus on a stimulus screen 57 cm from the eyes. Optical disks were plotted on the screen in order to estimate the approximate locations of the fovea. In visual stimulation runs, images were collected continuously as in the spontaneous runs. Each visual stimulus was presented for 1.5 s and separated by a 0.5 s inter-stimulus-interval. The beginning of each stimulus presentation was synchronized with the beginning of a frame scanning.

During the imaging session, slow drifts of cortex in the imaging field of view was observed. The drift was normally less than 100 μm in the X-Y plane and less than 80 μm along the Z-axis in a course of 6–8 hr. We frequently checked the cell features during the imaging and adjusted position of the focal plane accordingly. Drifts in the X-Y plane were further corrected in offline data analysis.

4.4. Visual stimuli

Visual stimuli were generated using ViSaGe (Cambridge Research Systems Ltd.) and presented on a 21-inch LCD monitor (Dell E1913SF) positioned 57 cm from the eyes. The stimulus screen was gamma corrected and worked at 60 Hz refreshing rate. Left- and right-eye visual fields were diverged by a pair of 9° prisms to prevent their overlap on the screen. A black board were placed between the two eyes to prevent cross eye stimulation. For black/white gratings, the luminance for white bars was 100 cd/ m^2 . Within each run, the stimuli were presented in a random order.

4.5. Stimuli for RF mapping

Circular grating patches sized 2.5° were presented at a grid of 5 \times 5 locations. Each grating had a rectangle waveform (duty cycle: 0.2; SF: 1.5 c/deg; TF: 8c/sec) and was presented at 4 different drifting directions (45°, 135°, 225°, 315°). Each stimulus was repeated for 3 times (total 5 \times 5 \times 4 \times 3 = 300 trials). RF positions were online analyzed and used for following stimulus presentation. Two eyes were mapped separately. The mapped population RF had an eccentricity of 3–5°.

4.6. Stimuli for estimating neuron's eye dominance

A 7°X7° grating patch was presented monocularly to the left or right eye. The mapped population RF locations for the two eyes were used here for the center locations of the square grating patch. Gratings are rectangle wave (duty cycle: 0.2; SF: 1.5 c/deg; TF: 8c/sec). Stimuli were presented in a block design. Each block contains 4 orientations (0°, 45°, 90°, 135°), two locations (for two eyes), as well as a blank condition (total 9 conditions). Gratings were drifting at random directions orthogonal to the gratings. Normally 20–30 blocks were presented.

4.7. Stimuli for estimating neuron's orientation preference

Similar to eye-dominance stimuli, grating patches were used for orientation test, except that the left- and right-eye stimuli were presented together through a full screen patch. Each block contains 17 conditions, including 8 orientations (in 22.5° steps), each drifting at two opposite directions, and a blank condition.

4.8. Stimuli for estimating neuron's color preference

Color stimuli were sinewave gratings ($SF = 0.15$ c/degrees, $TF = 1$ c/s) in full screen. Each block had 29 conditions, including 1 blank condition, and gratings in 7 different colors, each presented at 4 orientations (0° , 45° , 90° , 135°), drifting at one of the two directions randomly chosen orthogonal to the gratings. The 7 colors were: red (255,0,0), yellow (255,255,0), green (0,255,0), cyan (0,255,255), blue (0,0,255), purple (255,0,255) and white (255,255,255). The mean luminance for white gratings was 50 cd/m^2 , blue gratings were 7 cd/m^2 , and all other color gratings were 20 cd/m^2 .

5. Data analysis

5.1. Cell identification

We first did motion correction and cell identification with CalmAn toolbox v1.9.15 (Giovannucci et al., 2019) and Python v3.10.8, and obtained timecourses of fluorescent strength for individual neurons.

5.2. Preprocess

Each timecourse were first filtered with a Butterworth filter (5th order, 0.005Hz Highpass) to remove slow drifting background and breath noise. Then fluorescent change was calculated as $dF/F = (F-F_0)/F_0$, in which F_0 is the mean value of the lowest 10 % F values in the current run.

We did Z-score normalization for dF/F series before PCA, using $Z = \frac{dF - \bar{dF}}{\sigma_{dF}}$, in which dF is the dF/F of the current frame, \bar{dF} is the mean dF/F of the series, σ_{dF} is the standard deviation of the dF/F of the series.

5.3. Visual feature preference

Neuron's ocular dominance was evaluated using Cohen's D: $Cohen\ D = \frac{t}{\sqrt{N}}$, in which t is the t-test value for responses to the 4 left-eye stimuli and 4 right-eye stimuli, N is the number of samples.

Neuron's responses to 16 oriented gratings were fitted with a modified von Mises function (Mardia 1972): $y = a_0 + b_1 e^{c_1} \times \cos(\theta - \theta_{best}) + b_2 e^{c_2} \times \cos(\theta - \theta_{best} - \pi)$. Neurons had $R^2 > 0.7$ were considered had orientation preference and its preferred orientation was then obtained from this fitting function.

Neuron's color selectivity was evaluated by comparing its responses to each color grating and black-white grating (t-test). A t-value larger than 0 and $p < 0.05$ were considered had color selectivity to that color. Thus, a neuron can have more than one preferred color.

5.4. Functional maps

We obtained functional maps for ocular dominance, orientation, and color for each imaging sites. Each had two types: single-condition maps and difference maps. Use ocular dominance maps as example, there were two single-condition maps: left-eye condition map and right-eye condition map, each was obtained by calculating the mean of the Z-score for each cell. The difference map was a Cohen D map calculated using the Z-scores to left and right eye. For neurons' functional map, each neuron was simplified as a small disk in its original location and had a value calculated above.

5.5. Shuffled data

We used phased-shuffled spontaneous data as controls: each neuron's Z-score time series were first Fourier transformed and the phases were randomized. These frequency data were then transformed back to time series. These shuffled time series maintained the same power spectrum as original ones.

5.6. PCA

PCA (Principal Component Analysis) is a useful data-driven analysis tool and frequently used in fMRI research (Carbonell et al. 2011). For the spontaneous data, we used PCA to reduce its dimensionality in two separate ways. The first is illustrated in Fig. 2A, in which the dimension in Y-axis (cell dimension) was reduced. The second is illustrated in Fig. 4A, in which the dimension in X-axis (frame dimension) was reduced.

5.7. SVM classification based on PCA results

In order to examine the similarity between spontaneous frames and stimulus frames, we combined PCA and SVM classification. We first did PCA on spontaneous data to reduce the cell dimension. Then we plotted the frames obtained in stimulus conditions into the PC space. We used the coordinates in the first 10 dimensions to train a SVM classifier (scikit-learn toolbox, v1.3.0). Finally, spontaneous frames were classified in this trained SVM classifier.

5.8. Spontaneous maps

Based on the procedures above, we obtained spontaneous frames that resembles the stimulus-driven frames. A continuous sequence of classified frames was considered an "event". A spontaneous map can be calculated similarly as the one for stimulus frames.

5.9. Burstiness index

Following the methodology described by Wagenaar et al. (2005), we characterized the burstiness of both ensemble and single-cell activity by dividing the entire imaging sequence into 160 temporal windows. Specifically, we calculated the proportion of total events occurring in the top 15 % of windows with the highest event activity (24 windows in this case). The burstiness index (BI) was defined as $BI = (f_{15} - 0.15)/0.85$, where f_{15} represents the fraction of total events within these top 15 % windows. As expected under a uniform distribution, BI approaches zero, while higher BI values indicate greater temporal burstiness in spontaneous activity.

Data and code availability statement

Data used in this article can be find at <https://data.mendeley.com/datasets/v6563pxdn9/1>, and codes for data analysis is stored at <https://github.com/adolescent/Dynamic-Grouping-of-Ongoing-Activity-in-V1-Hypercolumns>.

CRedit authorship contribution statement

Rui Zhang: Writing – original draft, Visualization, Validation, Software, Project administration, Methodology, Investigation, Formal analysis, Data curation, Conceptualization. **Jiayu Wang:** Writing – original draft, Visualization, Validation, Project administration, Methodology, Investigation, Data curation, Conceptualization. **Xingya Cai:** Methodology, Investigation, Conceptualization. **Rendong Tang:** Methodology, Investigation. **Haidong D. Lu:** Writing – original draft, Validation, Supervision, Resources, Project administration, Methodology, Investigation, Funding acquisition, Data curation, Conceptualization.

Declaration of competing interest

The authors declare that they have no known competing financial interests or personal relationships that could have appeared to influence the work reported in this paper.

Acknowledgements

This work was supported by the National Science and Technology Innovation 2030 Major program (2022ZD0204600) and the National Natural Science Foundation of China (32271079, 31625012, and 31530029). We thank lab members J. Lu, Y. Xiao, for providing technical assistance.

Supplementary materials

Supplementary material associated with this article can be found, in the online version, at [doi:10.1016/j.neuroimage.2025.121157](https://doi.org/10.1016/j.neuroimage.2025.121157).

Data availability

<https://data.mendeley.com/datasets/v6563pxdn9/1> (An example dataset is available at Mendeley dataset.)

References

- Arieli, A., Shoham, D., Hildesheim, R., Grinvald, A., 1995. Coherent spatiotemporal patterns of ongoing activity revealed by real-time optical imaging coupled with single-unit recording in the cat visual cortex. *J. Neurophysiol.* 73 (5), 2072–2093. <https://doi.org/10.1152/jn.1995.73.5.2072>.
- Arieli, A., Sterkin, A., Grinvald, A., Aertsen, A., 1996. Dynamics of ongoing activity: explanation of the large variability in evoked cortical responses. *Science* (1979) 273, 1868–1871. <https://doi.org/10.1126/science.273.5283.1868>.
- Avitan, L., Stringer, C., 2022. Not so spontaneous multi-dimensional representations of behaviors and context in sensory areas. *Neuron* 110 (19), 3064–3075. <https://doi.org/10.1016/j.neuron.2022.06.019>.
- Cai, X., Xu, H., Han, C., Li, P., Wang, J., Zhang, R., Tang, R., Fang, C., Yan, K., Song, Q., Liang, C., Lu, H.D., 2023. Mesoscale functional connectivity in macaque visual areas. *Neuroimage* 271, 120019. <https://doi.org/10.1016/j.neuroimage.2023.120019>.
- Carbonell, F., Bellec, P., Shmuel, A., 2011. Global and system-specific resting-state fMRI fluctuations are uncorrelated: principal component analysis reveals anti-correlated networks. *Brain Connect.* 1 (6), 496–510. <https://doi.org/10.1089/brain.2011.0065>.
- Card, N.S., Gharabie, O.A., 2022. Cortical connectivity is embedded in resting state at columnar resolution. *Prog. Neurobiol.* 213, 102263. <https://doi.org/10.1016/j.pneurobio.2022.102263>.
- Ch'ng, Y.H., Reid, R.C., 2010. Cellular imaging of visual cortex reveals the spatial and functional organization of spontaneous activity. *Front. Integr. Neurosci.* 19 (4), 20. <https://doi.org/10.3389/fint.2010.00020> eCollection 2010.
- Chiu, C., Weliky, M., 2001. Spontaneous activity in developing ferret visual cortex in vivo. *J. Neurosci.* 21 (22), 8906–8914. <https://doi.org/10.1523/JNEUROSCI.21-22-08906.2001>.
- Fox, M.D., Raichle, M.E., 2007. Spontaneous fluctuations in brain activity observed with functional magnetic resonance imaging. *Nat. Rev. Neurosci.* 8, 700–711. <https://doi.org/10.1038/nrn2201>.
- Fukushima, M., Saunders, R.C., Leopold, D.A., Mishkin, M., Averbeck, B.B., 2012. Spontaneous high-gamma band activity reflects functional organization of auditory cortex in the awake macaque. *Neuron* 74, 899–910. <https://doi.org/10.1016/j.neuron.2012.04.014>.
- Gilbert, C.D., Wiesel, T.N., 1989. Columnar specificity of intrinsic horizontal and corticocortical connections in cat visual cortex. *J. Neurosci.* 9 (7), 2432–2442. <https://doi.org/10.1523/JNEUROSCI.09-07-02432.1989>.
- Giovannucci, A., Friedrich, J., Gunn, P., Kalfon, J., Brown, B.L., Koay, S.A., Taxidis, J., Najafi, F., Gauthier, J.L., Zhou, P., Khakh, B.S., Tank, D.W., Chklovskii, D.B., Pnevmatikakis, E.A., 2019. CalmAn an open source tool for scalable calcium imaging data analysis. *Elife* 17 (8), e38173. <https://doi.org/10.7554/elife.38173>.
- Goldberg, J.A., Rokni, U., Sompolinsky, H., 2004. Patterns of ongoing activity and the functional architecture of the primary visual cortex. *Neuron* 42 (3), 489–500. [https://doi.org/10.1016/s0896-6273\(04\)00197-7](https://doi.org/10.1016/s0896-6273(04)00197-7).
- Goltstein, P.M., Montijn, J.S., Pennartz, C.M.A., 2015. Effects of isoflurane anesthesia on ensemble patterns of Ca^{2+} activity in mouse v1: reduced direction selectivity independent of increased correlations in cellular activity. *PLoS. One* 10 (2), e0118277. <https://doi.org/10.1371/journal.pone.0118277>.
- Hubel, D.H., Wiesel, T.N., 1974. Uniformity of monkey striate cortex: a parallel relationship between field size, scatter, and magnification factor. *J. Comp. Neurol.* 158 (3), 295–305. <https://doi.org/10.1002/cne.901580305>.
- Kiani, R., Cueva, C.J., Reppas, J.B., Peixoto, D., Ryu, S.I., Newsome, W.T., 2015. Natural grouping of neural responses reveals spatially segregated clusters in prearcuate cortex. *Neuron* 85 (6), 1359–1373. <https://doi.org/10.1016/j.neuron.2015.02.014>.
- Kisvárdy, Z.F., Tóth, E., RauschM, Eysel UT, 1997. Orientation-specific relationship between populations of excitatory and inhibitory lateral connections in the visual cortex of the cat. *Cereb. Cortex* 7 (7), 605–618. <https://doi.org/10.1093/cercor/7.7.605>.
- Ko, H., Hofer, S.B., Pichler, B., Buchanan, K.A., Sjöström, P.J., Mrsic-Flogel, T.D., 2011. Functional specificity of local synaptic connections in neocortical networks. *Nature* 473 (7345), 87–91. <https://doi.org/10.1038/nature09880>.
- Ko, H., Cossell, L., Baragli, C., Antolik, J., Clopath, C., Hofer, S.B., Mrsic-Flogel, T.D., 2013. The emergence of functional microcircuits in visual cortex. *Nature* 496 (7443), 96–100. <https://doi.org/10.1038/nature12015>.
- Leopold, D.A., Murayama, Y., Logothetis, N.K., 2003. Very slow activity fluctuations in monkey visual cortex: implications for functional brain imaging. *Cereb. Cortex* 13 (4), 422–433. <https://doi.org/10.1093/cercor/13.4.422>.
- Livingstone, M., Hubel, D., 1984. Specificity of intrinsic connections in primate primary visual cortex. *J. Neurosci.* 4, 2830. <https://doi.org/10.1523/JNEUROSCI.04-11-02830.1984>.
- Luczak, A., McNaughton, B.L., Harris, K.D., 2015. Packet-based communication in the cortex. *Nat. Rev. Neurosci.* 16 (12), 745–755. <https://doi.org/10.1038/nrn4026>.
- Lund, J.S., Wu, C.Q., 1997. Local circuit neurons of macaque monkey striate cortex: IV. Neurons of laminae 1–3A. *J. Comp. Neurol.* 384 (1), 109–126. [https://doi.org/10.1002/\(sici\)1096-9861\(19970721\)384:1<109::aid-cne7>3.0.co;2-5](https://doi.org/10.1002/(sici)1096-9861(19970721)384:1<109::aid-cne7>3.0.co;2-5).
- Lund, J.S., Yoshioka, T., Levitt, J.B., 1993. Comparison of intrinsic connectivity in different areas of macaque monkey cerebral cortex. *Cereb. Cortex* 3 (2), 148–162. <https://doi.org/10.1093/cercor/3.2.148>, 1993 Mar-Apr.
- Maier, A., Adams, G.K., Aura, C., Leopold, D.A., 2010. Distinct superficial and deep laminar domains of activity in the visual cortex during rest and stimulation. *Front. Syst. Neurosci.* 10 (4), 31. <https://doi.org/10.3389/fnsys.2010.00031>.
- Malach, R., Amir, Y., Harel, M., Grinvald, A., 1993. Relationship between intrinsic connections and functional architecture revealed by optical imaging and in vivo targeted biocytin injections in primate striate cortex. *Proc. Natl. Acad. Sci.* 90, 10469–10473. <https://doi.org/10.1073/pnas.90.22.10469>.
- Mitra, A., Kraft, A., Wright, P., Acland, B., Snyder, A.Z., Rosenthal, Z., Raichle, M.E., 2018. Spontaneous infra-slow brain activity has unique spatiotemporal dynamics and laminar structure. *Neuron* 98 (2), 297–305. <https://doi.org/10.1016/j.neuron.2018.03.015>.
- Mizuno, H., Ikezoe, K., Nakazawa, S., Sato, T., Kitamura, K., Iwasato, T., 2018. Patchwork-type spontaneous activity in neonatal barrel cortex layer 4 transmitted via thalamocortical projections. *Cell Rep.* 22 (1), 123–135. <https://doi.org/10.1016/j.celrep.2017.12.012>.
- Mohajerani, M.H., Chan, A.W., Mohsenvand, M., LeDue, J., Liu, R., McVea, D.A., Murphy, T.H., 2013. Spontaneous cortical activity alternates between motifs defined by regional axonal projections. *Nature Neurosci.* 16 (10), 1426–1435. <https://doi.org/10.1038/nn.3499>.
- Mulholland, H.N., Hein, B., Kaschube, M., Smith, G.B., 2021. Tightly coupled inhibitory and excitatory functional networks in the developing primary visual cortex. *Elife* 10, e72456. <https://doi.org/10.7554/elife.72456>.
- Muta, K., Hata, J., Kawaguchi, N., Haga, Y., Yoshimaru, D., Hagiya, K., Kaneko, T., Miyabe-Nishiwaki, T., Komaki, Y., Seki, F., Okano, H.J., Okano, H., 2023. Effect of sedatives or anesthetics on the measurement of resting brain function in common marmosets. *Cereb. Cortex* 33 (9), 5148–5162. <https://doi.org/10.1093/cercor/bhac406>.
- Okun, M., Steinmetz, N., Cossell, L., Florencio Icaruso, M., Ko, H., Barthó, P., Moore, T., Hofer, S.B., Mrsic-Flogel, T.D., Carandini, M., Harris, K.D., 2015. Diverse coupling of neurons to populations in sensory cortex. *Nature* 521 (7553), 511–515. <https://doi.org/10.1038/nature14273>.
- Omer, D.B., Fekete, T., Ulchin, Y., Hildesheim, R., Grinvald, A., 2019. Dynamic patterns of spontaneous ongoing activity in the visual cortex of anesthetized and awake monkeys are different. *Cereb. Cortex* 29, 1291–1304. <https://doi.org/10.1093/cercor/bhy099>.
- See, J.Z., Atencio, C.A., Sohal, V.S., Schreiner, C.E., 2018. Coordinated neuronal ensembles in primary auditory cortical columns. *Elife* 7, e35587. <https://doi.org/10.7554/elife.35587>.
- Singh, G., Memoli, F., Ishkhanov, T., Sapiro, G., Carlsson, G., Ringach, D.L., 2008. Topological analysis of population activity in visual cortex. *J. Vis.* 8 (8), 1–18. <https://doi.org/10.1167/8.8.11>, 11.
- Smith, M.A., Kohn, A., 2008. Spatial and temporal scales of neuronal correlation in primary visual cortex. *J. Neurosci.* 28 (48), 12591–12603. <https://doi.org/10.1523/JNEUROSCI.2929-08.2008>.
- Smith, M.A., Sommer, M.A., 2013. Spatial and temporal scales of neuronal correlation in visual area V4. *J. Neurosci.* 33 (12), 5422–5432. <https://doi.org/10.1523/JNEUROSCI.4782-12.2013>.
- Smith, G.B., Hein, B., Whitney, D.E., Fitzpatrick, D., Kaschube, M., 2018. Distributed network interactions and their emergence in developing neocortex. *Nat. Neurosci.* 21, 1600–1608. <https://doi.org/10.1038/s41593-018-0247-5>.
- Stettler, D.D., Das, A., Bennett, J., Gilbert, C.D., 2002. Lateral connectivity and contextual interactions in macaque primary visual cortex. *Neuron* 36 (4), 739–750. [https://doi.org/10.1016/S0896-6273\(02\)01029-2](https://doi.org/10.1016/S0896-6273(02)01029-2).
- Stringer, C., Pachitariu, M., Steinmetz, N., Reddy, C.B., Carandini, M., Harris, K.D., 2019. Spontaneous behaviors drive multidimensional, brainwide activity. *Science* (1979) 364 (6437), eaav7893. <https://doi.org/10.1126/science.aav7893>.
- Tang, R., Song, Q., Li, Y., Zhang, R., Cai, X., Lu, H., 2020. Curvature-processing domains in primate V4. *Elife* 9, <https://doi.org/10.7554/elife.57502>.
- Tsodyks, M., Kenet, T., Grinvald, A., Arieli, A., 1999. Linking spontaneous activity of single cortical neurons and the underlying functional architecture. *Science* (1979) 286, 1943–1946. <https://doi.org/10.1126/science.286.5446.1943>.
- Vasireddi, A.K., Vazquez, A.L., Whitney, D.E., Fukuda, M., Kim, S.G., 2016. Functional connectivity of resting hemodynamic signals in submillimeter orientation columns of the visual cortex. *Brain Connect.* 6, 596–606. <https://doi.org/10.1089/brain.2015.0414>.

- Vincent, J.L., Patel, G.H., Fox, M.D., Snyder, A.Z., Baker, J.T., Van Essen, D.C., Zempel, J.M., Snyder, L.H., Corbetta, M., Raichle, M.E., 2007. Intrinsic functional architecture in the anaesthetized monkey brain. *Nature* 447, 83–86. <https://doi.org/10.1038/nature05758>.
- Wagenaar, D.A., Madhavan, R., Pine, J., Potter, S.M., 2005. Controlling bursting in cortical cultures with closed-loop multi-electrode stimulation. *J. Neurosci.* 25 (3), 680–688. <https://doi.org/10.1523/JNEUROSCI.4209-04.2005>.
- Yabuta, N.H., Callaway, E.M., 1998. Cytochrome-oxidase blobs and intrinsic horizontal connections of layer 2/3 pyramidal neurons in primate V1. *Vis. Neurosci.* 15, 1007–1027. <https://doi.org/10.1017/S0952523898156018>.
- Yoshioka, T., Blasdel, G.G., Levitt, J.B., Lund, J.S., 1996. Relation between patterns of intrinsic lateral connectivity, ocular dominance, and cytochrome oxidase-reactive regions in macaque monkey striate cortex. *Cereb. Cortex* 6, 297–310. <https://doi.org/10.1093/cercor/6.2.297>.